Energy Amplification of Streamwise Constant Channel Flow over Riblets

Shi Zhao [*] **Stephen Duncan** [**]

[*] *Department of Engineering Science, University of Oxford, UK*
(e-mail: shi.zhao@eng.ox.ac.uk).
[**] *Department of Engineering Science, University of Oxford, UK*
(e-mail: stephen.duncan@eng.ox.ac.uk).

Abstract: Riblets have been used as a passive method of reducing the drag of a fluid flowing over an airfoil. Riblets are structures that run parallel to one another that are positioned longitudinally to the flow. It has been shown experimentally that the drag coefficients over the surface can be reduced by up to 10% when the shape, spacing and height of the riblets are optimized. However, the mechanism of drag reduction is not fully understood. This paper investigates the effects of riblets on energy amplification in streamwise constant channel flow. The linearized Navier-Stokes equations are described by the two-dimensional/three-component model. The irregular domain is converted into a uniform one through a change of coordinates. Spectral methods are used to discretize these equations, leading to a finite-dimensional state space model. The transient growth and $\mathcal{H}_2$ norm of the flow system are calculated, which shows that the presence of riblets can reduce the transient growth and $\mathcal{H}_2$ norm of channel flow.

1. INTRODUCTION

The increasing cost of fuel and the need to reduce green house gas emissions have driven research into drag reduction techniques in many engineering disciplines. There are two types of drag reduction techniques available - active and passive techniques, and this paper focuses on a passive mechanism, which is the use of riblets. Experimental and numerical studies show that the introduction of riblet structures on the aerodynamic body results in significant reduction in drag (Walsh, 1983). This drag-reduction phenomenon is also widely observed in nature, for examples on shark skin and scallop shells (Bhushan, 2012). In the 1990's, tests on a scale model of an Airbus A320 cruising at Mach 0.7 showed reductions in viscous drag of 4.85% (Viswanath, 2002). Riblets have also been successfully used in applications other than aircrafts, for example on America's Cup racing yachts (Coustols and Savill, 1992), rowing skiffs and on the swimsuits used by the USA Olympic swimming team. Since the boundary layers in aircrafts are almost always turbulent, most studies have been focusing on investigating the effects of riblets on the drag reduction in turbulent flow (García-Mayoral and Jiménez, 2011). There has been less emphasis on the effects of riblets on laminar flow. It is reported in Choi et al. (1991) that drag reduction was not obtained in laminar flows over riblets and the net drag was increased. While the experimental and numerical studies in Djenidi et al. (1994) conclude that the drag was not increased in laminar boundary layer over riblets. Moreover, it has been shown experimentally that riblets can delay the laminar-turbulent transition and shift the transition downstream (Grek et al., 1996).

This paper considers the effects of riblets on energy amplification in laminar streamwise constant channel flow. Energy amplification has been identified as one possible explanation for the subcritical transition of channel flows (Schmid, 2007). It has been shown that due to the non-normality of the Orr-Sommerfeld operator, the flow can experience large energy amplification even when all the eigenvalues have negative real parts (Reddy and Henningson, 1993). The subcritical transition may be delayed if the presence of riblets can reduce the energy amplification in the laminar flow.

The analysis starts from the Navier-Stokes equations (NSE) of the flow over riblets. After linearizing about the steady state, a two-dimensional/three-component (2D/3C) model describing the streamwise invariant perturbation velocity field is derived. The reason for restricting our attention to streamwise independent flow modes is that it has been shown that in plane Poiseuille flow both the largest transient growth and maximal amplification of external excitations are identified at streamwise constant flow modes (Schmid and Henningson, 2001; Schmid, 2007). The advantage of the 2D/3C formulation is that no inversion of ill-conditioned operators is needed. The presence of riblets leads to an irregular domain, which is shifted to a space with smooth boundaries by a change of coordinates. The boundary conditions are also transformed to the new coordinate system. The infinite-dimensional system model is then discretized using a Chebyshev collocation method in the wall-normal direction and a Fourier Galerkin method in the spanwise direction. After obtaining the resulting finite-dimensional model of the linearized flow, the effects that how the introduction of riblets alters the transient growth and $\mathcal{H}_2$ norm are examined. Our results show that both the transient growth of most sensitive initial conditions and energy amplifications of stochastic forcing can be reduced by the presence of riblets. This suggests that the suppression of the energy amplification may delay the transition to turbulence, resulting in a reduction in drag.

The paper is organized as follows. Section 2 describes the governing equations of channel flow over riblets and obtains the steady state velocity profile. The equations modelling the perturbed flow are then linearized about the steady state and expressed in the 2D/3C form in Section 3. In Section 4, the ribbed domain is converted into a smooth domain by a transformation of coordinates and boundary conditions in the new coordinate system are derived. The semi-discrete (continuous in time and discrete in space) formulation of the model is obtained in Section 5 by discretizing the flow equations with spectral methods. The transient growth and $\mathcal{H}_2$ norm of the flow system are calculated in Section 6 and Section 7 concludes the paper.

Notation: A dot over a variable denotes its time derivative, superscripts ^{T} and * denote transpose and conjugate transpose, respectively. $[-1, 1]$ is the continuous set including the endpoints and all numbers between -1 and 1, while $\{-1, 1\}$ is the discrete set which includes only -1 and 1. We borrow some notation from MATLAB, such as `diag`, `chol` and `trace`.

2. EQUATIONS OF MOTION

We consider channel flow between two stationary plates. The geometry of the problem is shown in Fig. 1, where $\tilde{x}$, $\tilde{y}$ and $\tilde{z}$ are the coordinates of the streamwise, wall-normal and spanwise directions, respectively. The upper wall is a flat plate, while the lower wall is a plate with riblets aligned with the streamwise direction. The dimensions of the problem are normalized, so that the upper boundary of the flow occurs at the plate positioned at $\tilde{y} = 1$, while the lower boundary is at $\tilde{y} = -1 + f(\tilde{z})$ where $f(\tilde{z})$ describes the "shape" of the riblets. The analysis will be restricted to riblets that are aligned with the streamwise direction and are independent of $\tilde{x}$. The flow will be referred to as plane channel flow when both walls are smooth.
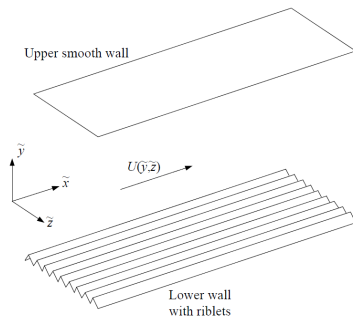
Fig. 1. Three-dimensional view of computational domain showing riblet structure on lower wall of channel.

The streamwise, wall-normal and spanwise components of the flow in the coordinate system $(\tilde{x}, \tilde{y}, \tilde{z})$ are denoted by $u(\tilde{x}, \tilde{y}, \tilde{z}, t)$, $v(\tilde{x}, \tilde{y}, \tilde{z}, t)$ and $w(\tilde{x}, \tilde{y}, \tilde{z}, t)$ respectively, and the non-dimensionalized NSE in this coordinate system are given by

$$\left(\frac{\partial}{\partial t} + u\frac{\partial}{\partial \tilde{x}} + v\frac{\partial}{\partial \tilde{y}} + w\frac{\partial}{\partial \tilde{z}} \right) u = -\frac{\partial p}{\partial \tilde{x}} + \frac{1}{\text{Re}}\tilde{\Delta} u \qquad (1)$$

$$\left(\frac{\partial}{\partial t} + u\frac{\partial}{\partial \tilde{x}} + v\frac{\partial}{\partial \tilde{y}} + w\frac{\partial}{\partial \tilde{z}} \right) v = -\frac{\partial p}{\partial \tilde{y}} + \frac{1}{\text{Re}}\tilde{\Delta} v \qquad (2)$$

$$\left(\frac{\partial}{\partial t} + u\frac{\partial}{\partial \tilde{x}} + v\frac{\partial}{\partial \tilde{y}} + w\frac{\partial}{\partial \tilde{z}} \right) w = -\frac{\partial p}{\partial \tilde{z}} + \frac{1}{\text{Re}}\tilde{\Delta} w \qquad (3)$$

$$\frac{\partial u}{\partial \tilde{x}} + \frac{\partial v}{\partial \tilde{y}} + \frac{\partial w}{\partial \tilde{z}} = 0 \qquad (4)$$

where

$$\tilde{\Delta} = \frac{\partial^2}{\partial \tilde{x}^2} + \frac{\partial^2}{\partial \tilde{y}^2} + \frac{\partial^2}{\partial \tilde{z}^2} \qquad (5)$$

and the Reynolds number Re is defined as

$$\text{Re} = \frac{\rho^\star U^\star h^\star}{\mu^\star} \qquad (6)$$

with $\rho^\star$ and $\mu^\star$ being the density and dynamic viscosity of the fluid, $h^\star$ is the length by which the wall-normal domain is normalized to $[-1 + f(\tilde{z}), 1]$, and $U^\star$ is the characteristic velocity induced by steady state streamwise pressure gradient $P_{\tilde{x}}^\star$

$$U^\star = -\frac{h^{\star 2} P_{\tilde{x}}^\star}{4\mu^\star} \qquad (7)$$

Note the star $\star$ is used to denote dimensional variables.

We seek a steady solution to this system of the form $(U, 0, 0)$ with no external forces, so that the NSE become

$$U\frac{\partial U}{\partial \tilde{x}} = -\frac{\partial P}{\partial \tilde{x}} + \frac{1}{\text{Re}}\tilde{\Delta} U \qquad (8)$$

$$0 = -\frac{\partial P}{\partial \tilde{y}} \qquad (9)$$

$$0 = -\frac{\partial P}{\partial \tilde{z}} \qquad (10)$$

$$\frac{\partial U}{\partial \tilde{x}} = 0 \qquad (11)$$

we can conclude that

$$\frac{\mathrm{d}P}{\mathrm{d}\tilde{x}} = \frac{1}{\text{Re}}\tilde{\Delta} U = -\frac{2}{\text{Re}} \qquad (12)$$

3. LINEARIZED EQUATIONS

We restrict our attention to streamwise constant perturbations. Redefining the flow as $(U + u, v, w, P + p)$ where $u(\tilde{y}, \tilde{z}, t), v(\tilde{y}, \tilde{z}, t), w(\tilde{y}, \tilde{z}, t)$ and $p(\tilde{y}, \tilde{z}, t)$ denote the velocity and pressure perturbations, and linearizing about the steady solution gives the 2D/3C model

$$\frac{\partial u}{\partial t} + v\frac{\partial U}{\partial \tilde{y}} + w\frac{\partial U}{\partial \tilde{z}} = \frac{1}{\text{Re}}\tilde{\Delta} u \qquad (13)$$

$$\frac{\partial v}{\partial t} = -\frac{\partial p}{\partial \tilde{y}} + \frac{1}{\text{Re}}\tilde{\Delta} v \qquad (14)$$

$$\frac{\partial w}{\partial t} = -\frac{\partial p}{\partial \tilde{z}} + \frac{1}{\text{Re}}\tilde{\Delta} w \qquad (15)$$

$$\frac{\partial v}{\partial \tilde{y}} + \frac{\partial w}{\partial \tilde{z}} = 0 \qquad (16)$$

Taking $\frac{\partial}{\partial \tilde{z}}$ of (14), $\frac{\partial}{\partial \tilde{y}}$ of (15) and eliminating the pressure terms gives

$$\frac{\partial}{\partial t}\left(\frac{\partial v}{\partial \tilde{z}} - \frac{\partial w}{\partial \tilde{y}} \right) = \frac{1}{\text{Re}}\tilde{\Delta}\left(\frac{\partial v}{\partial \tilde{z}} - \frac{\partial w}{\partial \tilde{y}} \right) \qquad (17)$$

Since v and w are related by the continuity equation (16), we can define a stream function $\psi(\tilde{y}, \tilde{z}, t)$ such that

$$\frac{\partial \psi}{\partial \tilde{z}}(\tilde{y}, \tilde{z}, t) = v(\tilde{y}, \tilde{z}, t) \tag{18}$$

$$\frac{\partial \psi}{\partial \tilde{y}}(\tilde{y}, \tilde{z}, t) = -w(\tilde{y}, \tilde{z}, t) \tag{19}$$

Now (17) can be rewritten as

$$\frac{\partial}{\partial t} \tilde{\Delta} \psi = \frac{1}{\mathrm{Re}} \tilde{\Delta}^2 \psi \tag{20}$$

Equations (13) and (18)-(20) can be combined to give

$$\mathcal{E}\dot{\mathbf{x}} = \mathcal{A}\mathbf{x} \tag{21}$$

$$\mathbf{y} = \mathcal{C}\mathbf{x} \tag{22}$$

where $\mathbf{x} = [u\ \psi]^T$, $\mathbf{y} = [u\ v\ w]^T$, and

$$\mathcal{E} = \begin{bmatrix} 1 & 0 \\ 0 & \tilde{\Delta} \end{bmatrix} \tag{23}$$

$$\mathcal{A} = \begin{bmatrix} \dfrac{1}{\mathrm{Re}}\tilde{\Delta} & \dfrac{\partial U}{\partial \tilde{z}}\dfrac{\partial}{\partial \tilde{y}} - \dfrac{\partial U}{\partial \tilde{y}}\dfrac{\partial}{\partial \tilde{z}} \\ 0 & \dfrac{1}{\mathrm{Re}}\tilde{\Delta}^2 \end{bmatrix} \tag{24}$$

$$\mathcal{C} = \begin{bmatrix} 1 & 0 \\ 0 & \dfrac{\partial}{\partial \tilde{z}} \\ 0 & -\dfrac{\partial}{\partial \tilde{y}} \end{bmatrix} \tag{25}$$

As in plane channel flow, the perturbations are assumed to be periodic in the spanwise direction, with no-slip conditions at solid boundaries, i.e.,

$$u|_{\tilde{y}=1} = v|_{\tilde{y}=1} = w|_{\tilde{y}=1} = 0 \tag{26}$$

$$u|_{\tilde{y}=-1+f(\tilde{z})} = v|_{\tilde{y}=-1+f(\tilde{z})} = w|_{\tilde{y}=-1+f(\tilde{z})} = 0 \tag{27}$$

4. TRANSFORMATION OF COORDINATES

Spectral methods are used to discretize the resulting governing equations with all operators replaced by appropriate differentiation matrices. One problem with this approach is the poor accuracy and efficiency of spectral methods on irregular domains (Boyd, 2001). To circumvent this difficulty, we apply the following change of coordinates (Orszag, 1980)

$$x = \tilde{x}, \quad y = F(\tilde{y}, \tilde{z}) = \frac{2\tilde{y} - f(\tilde{z})}{2 - f(\tilde{z})}, \quad z = \tilde{z} \tag{28}$$

which has the effect of mapping $\tilde{y} \in [-1 + f(\tilde{z}), 1]$ to $y \in [-1, 1]$. Note that

$$\frac{\partial}{\partial \tilde{y}} = \frac{\partial \tilde{x}}{\partial \tilde{y}}\frac{\partial}{\partial x} + \frac{\partial F}{\partial \tilde{y}}\frac{\partial}{\partial y} + \frac{\partial \tilde{z}}{\partial \tilde{y}}\frac{\partial}{\partial z} = \frac{\partial F}{\partial \tilde{y}}\frac{\partial}{\partial y} \tag{29}$$

$$\frac{\partial}{\partial \tilde{z}} = \frac{\partial \tilde{x}}{\partial \tilde{z}}\frac{\partial}{\partial x} + \frac{\partial F}{\partial \tilde{z}}\frac{\partial}{\partial y} + \frac{\partial \tilde{z}}{\partial \tilde{z}}\frac{\partial}{\partial z} = \frac{\partial}{\partial z} + \frac{\partial F}{\partial \tilde{z}}\frac{\partial}{\partial y} \tag{30}$$

where $\frac{\partial F}{\partial \tilde{y}} = \frac{2}{2 - f(z)}$, $\frac{\partial F}{\partial \tilde{z}} = \frac{(y-1)f'(z)}{2 - f(z)}$ with $f'(z)$ being the first derivative of $f(z)$ with respect to z. All the operators can be transformed into the new coordinates in the same manner, although the expressions are rather cumbersome.

The boundary conditions (26) and (27) can now be transformed to

$$u|_{y=\pm 1} = v|_{y=\pm 1} = w|_{y=\pm 1} = 0 \tag{31}$$

From the boundary conditions of w, we have

$$\left.\frac{\partial \psi}{\partial \tilde{y}}\right|_{y=\pm 1} = \left.\frac{\partial F}{\partial \tilde{y}}\frac{\partial \psi}{\partial y}\right|_{y=\pm 1} = 0 \tag{32}$$

which means that

$$\left.\frac{\partial \psi}{\partial y}\right|_{y=\pm 1} = 0 \tag{33}$$

Similarly, from the boundary conditions of v,

$$\left.\frac{\partial \psi}{\partial \tilde{z}}\right|_{y=\pm 1} = \left.\left[\frac{\partial \psi}{\partial z} + \frac{\partial F}{\partial \tilde{z}}\frac{\partial \psi}{\partial y}\right]\right|_{y=\pm 1} = 0 \tag{34}$$

which together with (33) yields

$$\left.\frac{\partial \psi}{\partial z}\right|_{y=\pm 1} = 0 \tag{35}$$

Due to the assumption that the velocity field is periodic in the spanwise direction, this condition leads to

$$\psi|_{y=\pm 1} = 0 \tag{36}$$

To sum up, in the new coordinate system, both u and ψ satisfy homogeneous Dirichlet boundary conditions, while ψ also satisfies homogeneous Neumann boundary conditions.

5. SEMI-DISCRETE FORMULATION

The riblet structure is taken to be periodic in the z (and $\tilde{z}$) direction with period $2\pi/\gamma$. It is assumed that the steady-state flow $U(y, z)$, which is described by the Poisson equation

$$\tilde{\Delta}U = -2 \tag{37}$$

and the perturbation velocity field are both periodic in z direction with wavenumber β. Since the period of the velocity field must be an exact multiple of that of the riblets, $Q = \gamma/\beta$ is an integer.

We normalize the spanwise domain $[0, 2\pi/\beta]$ to $[0, 2\pi]$, then in the normalized domain, the variables can be expressed as Fourier series such as

$$v(y, z, t) = \sum_{n=-\infty}^{\infty} \hat{v}_n(y, t)\mathrm{e}^{\mathrm{i}nz} \tag{38}$$

$$f(z) = \sum_{n=-\infty}^{\infty} \hat{f}_n \mathrm{e}^{\mathrm{i}nz} \tag{39}$$

and $\hat{f}_n = 0$ for all $n \neq mQ$ where m is an integer. When the spacing between riblets is small, as is usually the case for flow with high Reynolds numbers, then Q is large, which means that only coefficients $\hat{f}_n$ for values of n that are multiples of Q are nonzero, and this sparsity is exploited in the solution of the problem.

The steady flow U can be solved numerically by discretizing (37) using a Chebyshev collocation method in the y direction and a Fourier Galerkin method in the z direction. In the new coordinate system, the Laplacian operator $\tilde{\Delta}$ becomes

$$\tilde{\Delta} = K_1 \frac{\partial}{\partial y} + K_2 \frac{\partial^2}{\partial y \partial z} + K_3 \frac{\partial^2}{\partial y^2} + K_4 \frac{\partial^2}{\partial z^2} \tag{40}$$

where the expressions $K_i(y, z), i \in \{1, 2, 3, 4\}$ are known and can be expressed in terms of Fourier series

$$K_i(y, z) = \sum_{n=-\infty}^{\infty} \hat{k}_n^{(i)}(y) \, e^{inz} \tag{41}$$

Moreover, it can be shown that $\hat{k}_n^{(i)}(y)$ is nonzero only when n is an exact multiple of Q.

Using these expansions in (37), applying the convolution theorem for Fourier series and rearranging leads to

$$\sum_{n=-\infty}^{\infty} e^{inz} \sum_{m=-\infty}^{\infty} \hat{k}_{n-m}^{(3)}(y) \frac{d^2 \hat{U}_m}{dy^2} + \left[\hat{k}_{n-m}^{(1)}(y) + \right.$$
$$\left. im \, \hat{k}_{n-m}^{(2)}(y) \right] \frac{d\hat{U}_m}{dy} - m^2 \hat{k}_{n-m}^{(4)}(y) \, \hat{U}_m(y) = -2 \tag{42}$$

Defining an inner product as

$$\langle p(y, z) q(y, z) \rangle = \int_0^{2\pi} p^*(y, z) \, q(y, z) dz \tag{43}$$

and taking the inner product of the expression in (42) with a Galerkin test function $e^{i\ell z}$, where the summation is limited to $2M + 1$ terms, we have

$$2\pi \sum_{m=-M}^{M} \hat{k}_{\ell-m}^{(3)}(y) \frac{d^2 \hat{U}_m}{dy^2} + \left[\hat{k}_{\ell-m}^{(1)}(y) + im \, \hat{k}_{\ell-m}^{(2)}(y) \right] \frac{d\hat{U}_m}{dy}$$
$$- m^2 \hat{k}_{\ell-m}^{(4)}(y) \, \hat{U}_m(y) = b_\ell \tag{44}$$

where

$$b_\ell = \begin{cases} -4\pi & \text{for } \ell = 0 \\ 0 & \text{for } \ell \neq 0 \end{cases} \tag{45}$$

which represents $2M + 1$ coupled second order, ordinary differential equations. The values of $\hat{U}_m(y)$ can be solved numerically at the Chebyshev Gauss Lobatto points on $y \in [-1, 1]$ by stacking the values of $\hat{U}_m(y)$ at N sample points into a vector $\hat{\mathbf{U}} \in \mathbb{C}^{(2M+1)N}$, so that

$$\hat{\mathbf{U}} = \begin{bmatrix} \hat{\mathbf{U}}_{-M} & \dots & \hat{\mathbf{U}}_{-1} & \hat{\mathbf{U}}_0 & \hat{\mathbf{U}}_1 & \dots \hat{\mathbf{U}}_M \end{bmatrix}^T \tag{46}$$

where $\hat{\mathbf{U}}_m \in \mathbb{C}^N$ are the samples of $U_m(y)$ at the N Chebyshev points. The discretized version of the coupled ODE's in (44) take the form $\tilde{\mathbf{\Delta}}\hat{\mathbf{U}} = \mathbf{b}$ where $\mathbf{b} \in \mathbb{C}^{(2M+1)N}$ contains the terms b_ℓ. The matrix $\tilde{\mathbf{\Delta}} \in \mathbb{C}^{(2M+1)N \times (2M+1)N}$ consists of a series of blocks $[\tilde{\mathbf{\Delta}}]_{\ell,m} \in \mathbb{C}^{N \times N}$, that satisfy

$$[\tilde{\mathbf{\Delta}}]_{\ell,m} = \mathtt{diag}\left\{ \hat{\mathbf{k}}_{\ell-m}^{(3)} \right\} \mathbf{D}_N^2 + \mathtt{diag}\left\{ \hat{\mathbf{k}}_{\ell-m}^{(1)} + im \, \hat{\mathbf{k}}_{\ell-m}^{(2)} \right\} \mathbf{D}_N$$
$$- \mathtt{diag}\left\{ m^2 \hat{\mathbf{k}}_{\ell-m}^{(4)} \right\} \tag{47}$$

where $\mathbf{D}_N \in \mathbb{R}^{N \times N}$ and $\mathbf{D}_N^2 \in \mathbb{R}^{N \times N}$ are the first and second order Chebyshev differentiation matrices with the homogeneous Dirichlet boundary conditions imposed on, respectively, and $\hat{\mathbf{k}}_{\ell-m}^{(i)} \in \mathbb{C}^N$ are vectors obtained by sampling $\hat{k}_{\ell-m}^{(i)}(y)$ at the Chebyshev points.

The key point is that because $\hat{k}_{\ell-m}^{(i)}(y)$ is only nonzero when $\ell - m$ is an exact multiple of Q, the $\tilde{\mathbf{\Delta}}$ matrix has the structure shown in Figure 2(a), where each of the individual blocks has dimension N by N. By rearranging the order of the terms in $\hat{\mathbf{U}}$, the structure of the $\tilde{\mathbf{\Delta}}$ matrix can be arranged into the block diagonal form shown in Figure 2(b), which consists of Q blocks.
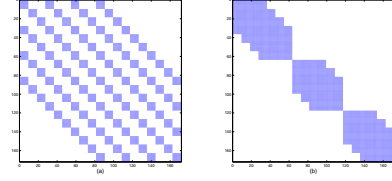
Fig. 2. Structure of $\tilde{\mathbf{\Delta}}$ matrix (a) before rearranging (b) after rearranging

Equations (21)-(22) can be discretized via the same methods that were used to solve the steady solution U, although the implementation is more laborious. Chebyshev differentiation matrices implemented by Weideman & Reddy (Weideman and Reddy, 2000) are used in the calculation. Then a finite-dimensional state space model of the linearized flow can be expressed as

$$\mathbf{E}\dot{\hat{\mathbf{x}}} = \mathbf{A}\hat{\mathbf{x}} \tag{48}$$

$$\hat{\mathbf{y}} = \mathbf{C}\hat{\mathbf{x}} \tag{49}$$

where $\mathbf{E}, \mathbf{A}$ and $\mathbf{C}$ are the discretized versions of the corresponding operators. $\hat{\mathbf{x}}$ and $\hat{\mathbf{y}}$ are vectors stacking the values of Fourier coefficients of $\mathbf{x}$ and $\mathbf{y}$ at the sample points, respectively. The matrices can also be made block diagonal by rearranging the structures. Since $\mathbf{E}$ is well-conditioned, it is possible to invert the matrix without introducing non-negligible errors. Now we are able to describe the system with the standard state space representation

$$\dot{\hat{\mathbf{x}}} = \hat{\mathbf{A}}\hat{\mathbf{x}} \tag{50}$$

$$\hat{\mathbf{y}} = \hat{\mathbf{C}}\hat{\mathbf{x}} \tag{51}$$

with $\hat{\mathbf{A}} = \mathbf{E}^{-1}\mathbf{A}$ and $\hat{\mathbf{C}} = \mathbf{C}$.

The kinetic energy density of the perturbation is defined as

$$E = \frac{1}{2} \int_{\tilde{z}=0}^{\tilde{z}=2\pi} \int_{\tilde{y}=-1+f(\tilde{z})}^{\tilde{y}=1} \left(u^2 + v^2 + w^2 \right) d\tilde{y} d\tilde{z} \tag{52}$$

which in the new coordinate system is

$$E = \frac{1}{2} \int_{z=0}^{z=2\pi} \int_{y=-1}^{y=1} \left(u^2 + v^2 + w^2 \right) \left(\frac{1}{\frac{\partial F}{\partial \tilde{y}}} \right) dy dz \tag{53}$$

and in the discrete formulation becomes

$$E = \hat{\mathbf{y}}^* \hat{\mathbf{W}}_{\mathbf{y}} \hat{\mathbf{y}} = \hat{\mathbf{x}}^* \hat{\mathbf{C}}^* \hat{\mathbf{W}}_{\mathbf{y}} \hat{\mathbf{C}} \hat{\mathbf{x}} \tag{54}$$

Defining $\hat{\mathbf{W}}_{\mathbf{x}} = \hat{\mathbf{C}}^* \hat{\mathbf{W}}_{\mathbf{y}} \hat{\mathbf{C}}$ and $\hat{\mathbf{F}}_{\mathbf{x}} = \mathtt{chol}(\hat{\mathbf{W}}_{\mathbf{x}})$, the energy norm and the standard Euclidean norm of vector $\hat{\mathbf{x}}$ is related by $\|\hat{\mathbf{x}}\|_E = \|\hat{\mathbf{F}}_{\mathbf{x}}\hat{\mathbf{x}}\|_2$. Similarly, denote $\hat{\mathbf{F}}_{\mathbf{y}} = \mathtt{chol}(\hat{\mathbf{W}}_{\mathbf{y}})$, then $\|\hat{\mathbf{y}}\|_E = \|\hat{\mathbf{F}}_{\mathbf{y}}\hat{\mathbf{y}}\|_2$. By a change of variables $\check{\mathbf{x}} = \hat{\mathbf{F}}_{\mathbf{x}}\hat{\mathbf{x}}$ and $\check{\mathbf{y}} = \hat{\mathbf{F}}_{\mathbf{y}}\hat{\mathbf{y}}$, the representation of the system can be transformed to

$$\dot{\check{\mathbf{x}}} = \check{\mathbf{A}}\check{\mathbf{x}} \tag{55}$$

$$\check{\mathbf{y}} = \check{\mathbf{C}}\check{\mathbf{x}} \tag{56}$$

with $\check{\mathbf{A}} = \hat{\mathbf{F}}_{\mathbf{x}}\hat{\mathbf{A}}\hat{\mathbf{F}}_{\mathbf{x}}^{-1}$ and $\check{\mathbf{C}} = \hat{\mathbf{F}}_{\mathbf{y}}\hat{\mathbf{C}}\hat{\mathbf{F}}_{\mathbf{x}}^{-1}$.

The discretization resolutions used to obtain the results reported in the following section were checked to ensure that they are sufficiently high.

6. EFFECTS OF RIBLETS ON ENERGY AMPLIFICATION

In the remainder of the paper we shall consider sinusoidal riblets which take the form $f(z) = \kappa \sin(\gamma z)$, although the analysis is generally applicable to any riblet whose shape function is fourth differentiable. The dimensionless steady state velocity profile $U(\tilde{y}, \tilde{z})$ at $\gamma = 8$ and $\kappa = 0.04$ is depicted in Fig. 3.
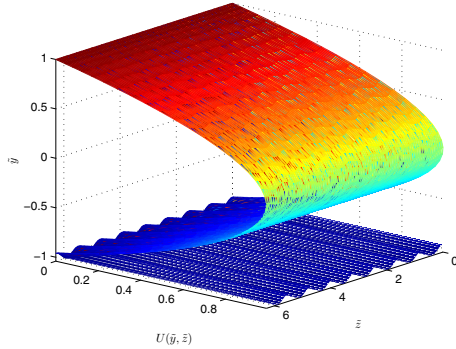
Fig. 3. Steady state velocity profile of channel flow over riblets, $\gamma = 8, \kappa = 0.04$

6.1 Most Unstable Eigenvalues

In order to see how the presence of riblets alters the linear stability of the flow system, the eigenvalues of $\hat{\mathbf{A}}$ are calculated. Due to the structure of operator $\mathcal{A}$, change of Reynolds number Re only scales the eigenvalues. Therefore it suffices to compute the eigenvalues at one Reynolds number. The time of calculating the eigenvalues and eigenvectors of $\hat{\mathbf{A}}$ is reduced by a factor of roughly Q^2 due to the sparsity of the matrix. Fig. 4 plots the eigenvalue with largest real part Λ against Q at Re $= 600, \beta = 2, \kappa = 0.02$. As a comparison, the most unstable eigenvalue in the absence of riblets is $\Lambda_c = -4.112 \times 10^{-3}$, which is shown in the red line.
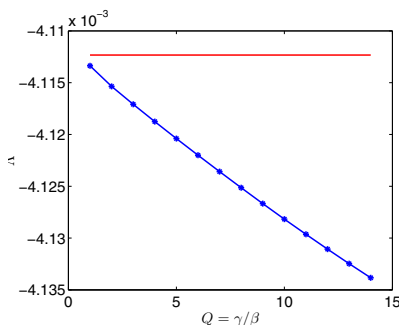
Fig. 4. Effects of riblets on Λ, Re $= 600, \beta = 2, \kappa = 0.02$.

Note that $Q = \gamma/\beta$ stands for the number of riblets within one period of perturbation velocity field. It therefore means that in the case considered, the smaller the riblet spacing, the more linearly stable the flow.

6.2 Transient Growth without External Forcing

In this subsection, the effects of riblets on the transient energy growth of the linearized channel flow are investi-

gated. It is now well known that although the streamwise constant plane channel flow is always linearly stable, due to the nonnormality of the Orr-Sommerfeld operator, with certain initial perturbations, the kinetic energy of the flow can grow rapidly before decaying eventually and this phenomenon is known as transient growth (Schmid, 2007). It has been identified that the streamwise constant flow is the modes which can have the largest transient growth (Schmid and Henningson, 2001). The largest possible energy amplification factor is shown to behave like $O(\text{Re}^2)$ in plane channel flow (Reddy and Henningson, 1993).

The maximal energy amplification factor at time t is defined as

$$G(t) = \sup_{\check{\mathbf{x}}_0 \neq 0} \frac{\|\check{\mathbf{x}}(t)\|_2^2}{\|\check{\mathbf{x}}_0\|_2^2} = \|\exp(\check{\mathbf{A}}t)\|_2^2 = \|\hat{\mathbf{F}}_{\mathbf{x}} \exp(\hat{\mathbf{A}}t) \hat{\mathbf{F}}_{\mathbf{x}}^{-1}\|_2^2 \tag{57}$$

and it is essentially an optimization over all initial conditions. For ease of reference, we define $G = \sup_t G(t)$, which is an optimization over time t.

Denote G_c as the maximal amplification factor G for streamwise constant plane Poiseuille flow at Re $= 600, \beta = 2$, it is straightforward to use the methods specified in Schmid and Henningson (2001) to obtain $G_c \approx 70.772$, which occurs at $t \approx 46$. Note that this value can also be obtained by setting $\kappa = 0$ and carrying out the computation described previously. The relative error is of order 10^{-7}. We use G_c as a benchmark to check how G is changed by the presence of riblets with $\kappa = 0.02$. To reduce the computing time, a number of most stable eigenmodes of $\hat{\mathbf{A}}$ are discarded in the calculation. This strategy was employed in Reddy and Henningson (1993) and the details can be found in Schmid and Henningson (2001). The result is illustrated in Fig. 5, where $(G/G_c - 1) \times 100$ is plotted against Q.
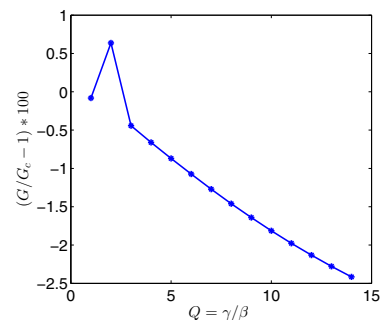
Fig. 5. Effects of riblets on G, Re $= 600, \beta = 2, \kappa = 0.02$.

As can be seen, the presence of sinusoidal riblets can indeed reduce G with the exception at $Q = 2$. The percentage of reduction is monotonically increasing with Q between 2 and 14, suggesting that the smaller the spacing of riblet is, the smaller G is. The calculation for larger Q is very expensive and therefore is not carried out here.

What is interesting is that at $Q = 2$, although $\Lambda < \Lambda_c$, G is larger than G_c. A closer examination reveals that the second rightmost eigenvalue of $\hat{\mathbf{A}}$ at $Q = 2$ is increased by riblets. While for other Q, this particular eigenvalue is decreased. This might be the reason that G is increased at $Q = 2$.

The behavior of G at Re = 1000 is very similar to that at Re = 600, although the exact percentages of reduction are not identical. This is probably because the change of eigenvalues by riblets has a dominant effect on G.

Our computation shows that G decreases with increasing κ, but it should be noted that κ should be reasonably small, otherwise the laminar pressure gradient will be changed and the model will no longer be valid.

6.3 Energy Amplification with Stochastic Forcing

This subsection is concerned with the energy amplification of the fluid flow system subject to stochastic forcing which models background noise. For simplicity, the energy of the noise is assumed to be unity. Studies of energy amplification of stochastic forcing in plane channel flow were conducted in Butler and Farrell (1992) and Bamieh and Dahleh (2001). It has been shown analytically that the energy amplification of streamwise constant channel flow with stochastic excitation can be as high as $O(\text{Re}^3)$. The situation is more involved with the presence of riblets and the analysis here is carried out numerically.

Since we assume that the stochastic forcing has unit energy, the model of system (55)-(56) becomes

$$\dot{\check{\mathbf{x}}} = \check{\mathbf{A}}\check{\mathbf{x}} + \check{\mathbf{d}}_{\mathbf{w}} \tag{58}$$

$$\check{\mathbf{y}} = \check{\mathbf{C}}\check{\mathbf{x}} \tag{59}$$

The energy amplification factor of the system is given by $\texttt{trace}(\check{\mathbf{C}}\check{\boldsymbol{\Omega}}\check{\mathbf{C}}^*)$ with $\check{\boldsymbol{\Omega}}$ being the controllability grammian, which is the solution of the Lyapunov equation

$$\check{\mathbf{A}}\check{\boldsymbol{\Omega}} + \check{\boldsymbol{\Omega}}\check{\mathbf{A}}^* = -\mathbf{I} \tag{60}$$

where $\mathbf{I}$ is an identity matrix. Using the identities of matrix trace, it is not difficult to verify that $\texttt{trace}(\check{\mathbf{C}}\check{\boldsymbol{\Omega}}\check{\mathbf{C}}^*) = \texttt{trace}(\check{\boldsymbol{\Omega}})$.

The square root of $\texttt{trace}(\check{\boldsymbol{\Omega}})$ is the $\mathcal{H}_2$ norm of the system. By comparing the $\mathcal{H}_2$ norms of channel flow over riblets and over flat plates, we can see how the riblets affect the energy amplification. Denote T as $\sqrt{\texttt{trace}(\check{\boldsymbol{\Omega}})}$ at $\kappa = 0.02, \text{Re} = 600, \beta = 2$ and T_c as the value without riblets. Fig. 6 shows that riblets have the effect of suppressing the $\mathcal{H}_2$ norm of the system. Unlike transient growth, the $\mathcal{H}_2$ norm is reduced for all Q considered.
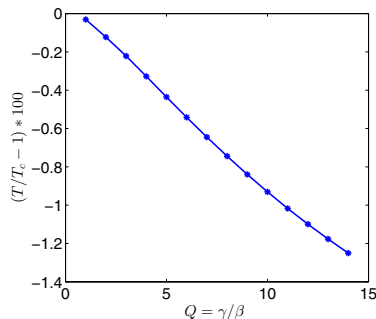
Fig. 6. Effects of riblets on T, Re = 600, $\beta = 2$, $\kappa = 0.02$.

7. CONCLUDING REMARKS

This paper shows that the introduction of riblets can suppress the transient growth of the most sensitive initial conditions and energy amplification of stochastic forcing in linearized channel flow. Since transient growth and energy amplification have been identified as the possible explanations for subcritical transition of channel flow, their suppression could be the reason for the delay of laminar-turbulent transition of the flow over riblets.

ACKNOWLEDGEMENTS

REFERENCES

Bamieh, B. and Dahleh, M. (2001). Energy amplification in channel flows with stochastic excitation. *Physics of Fluids*, 13(11), 3258–3269.

Bhushan, B. (2012). Shark skin surface for fluid-drag reduction in turbulent flow. In *Biomimetics*, 227–265. Springer.

Boyd, J.P. (2001). *Chebyshev and Fourier Spectral Methods,Second Edition*. Dover Publications,Inc., New York.

Butler, K.M. and Farrell, B.F. (1992). Three-dimensional optimal perturbations in viscous shear flow. *Physics of Fluids A*, 4(8), 1637–1650.

Choi, H., Moin, P., and Kim, J. (1991). On the effects of riblets in fully developed laminar channel flows. *Physics of Fluids*, 3(8), 1892–1896.

Coustols, E. and Savill, A. (1992). Turbulent skin-friction drag reduction by active and passive means. part 1. everything you wanted to know about riblets, lebus and other devices. Technical report, DTIC Document.

Djenidi, L., Anselmet, F., Liandrat, J., and Fulachier, L. (1994). Laminar boundary layer over riblets. *Physics of Fluids*, 6(9), 2993–2999.

García-Mayoral, R. and Jiménez, J. (2011). Drag reduction by riblets. *Philosophical Transactions of the Royal Society A: Mathematical, Physical and Engineering Sciences*, 369(1940), 1412–1427.

Grek, G., Kozlov, V., and Titarenko, S. (1996). An experimental study of the influence of riblets on transition. *Journal of Fluid Mechanics*, 315, 31–50.

Orszag, S.A. (1980). Spectral methods for problems in complex geometries. *Journal of Computational Physics*, 37(1), 70–92.

Reddy, S.C. and Henningson, D.S. (1993). Energy growth in viscous channel flows. *Journal of Fluid Mechanics*, 252, 209–238.

Schmid, P.J. and Henningson, D.S. (2001). *Stability and Transition in Shear Flows*. Springer-Verlag Inc., New York.

Schmid, P.J. (2007). Nonmodal stability theory. *Annual Review of Fluid Mechanics*, 39, 139–162.

Viswanath, P. (2002). Aircraft viscous drag reduction using riblets. *Progress in Aerospace Sciences*, 38(6), 571–600.

Walsh, M.J. (1983). Riblets as a viscous drag reduction technique. *AIAA Journal*, 21(4), 485–486.

Weideman, J.A. and Reddy, S.C. (2000). A Matlab differentiation matrix suite. *ACM Transactions on Mathematical Software*, 26, 465–519.